



Shake table tests of a corrugated steel sheathed cold-formed steel structure

Yan Zhao ^a, Cheng Yu ^b, Wenyng Zhang ^{a,*}, Zhiqiang Xie ^c, Shaole Yu ^d, Xiuli Du ^a

^a Beijing Key Laboratory of Earthquake Engineering and Structural Retrofit, Beijing University of Technology, Beijing, China

^b Department of Engineering Technology, University of North Texas, Denton, TX, United States

^c School of Civil and Transportation Engineering, Beijing University of Civil Engineering and Architecture, Beijing, China

^d China Construction Eighth Engineering Division Co., Ltd., Shanghai, 200135, China



ARTICLE INFO

Keywords:

Cold-formed steel
Corrugated steel sheathing
Seismic performance
Shake table tests
Dynamic properties

ABSTRACT

The corrugated steel sheathed cold-formed steel (CFS) shear wall is an innovative lateral force-resistant system with excellent potential for development. Many research has been conducted on the seismic behavior of this innovative shear wall system. However, dynamic properties as well as the failure mechanism of the CFS structures with corrugated steel sheathing are still unclear. This study aimed to increase knowledge of the seismic performance of CFS structures through the shaking table test, of which the seismic force resisting system was provided by corrugated steel sheathed shear walls. Importantly, this test also took into account the extremely rare precautionary intensity. The main results indicated that damage of CFS structure began to occur in the walls and floors under rare earthquakes and increased further with the seismic intensity. The final damage primarily occurred through the failure of connections and inner panels under extremely rare precautionary intensity. The degree of variation in the dynamic properties of the structure increased further as the damage accumulated. In particular, the damping ratio of the structure in the non-linear phase ranged from 5% to 7.5%. It was unreasonable to assume that the trend of the acceleration amplification factor with structural height was determined as a linear relationship. The peak inter-story drift ratio of the corrugated steel sheathing CFS structure could meet the multi-level seismic precaution requirements of the code. Finally, the seismic performance parameters of the CFS structure were evaluated by numerical simulations. This research will provide a reference for the seismic design of CFS structures under extremely rare conditions.

1. Introduction

Cold-formed steel (CFS) structures have been widely used in low-rise residential and commercial buildings in North America, Australia, and New Zealand. The shear wall is an important element of CFS systems. One of the main factors impacting the structural performance of CFS shear walls is the sheathing material. Extensive experimental research has been performed on the shear resistance of CFS framed shear walls with various sheathing materials under both monotonic and cyclic loading. Tarpy [1], Girard [2], Serrette et al. [3,4], and Salenikovich et al. [5] have investigated the effects of sheathing materials such as plywood, oriented strand board (OSB), gypsum board, fiber bond wallboard (FB), and fireproof board in sheathed walls under monotonic and cyclic loading. Liu et al. [6] examined the behavior of CFS double-sided board wall (the exterior OSB and the interior gypsum panels) through shear tests. The

* Corresponding author.

E-mail address: wenyingchangan@163.com (W. Zhang).

impact of configuration of horizontal and vertical seams, presence of a ledger, field stud thickness and wall aspect ratio were also studied. Steel-sheathed CFS shear walls were experimentally investigated by Yu [7]. The main failure mode of the shear wall was determined, and the nominal shear strengths for wind load and seismic load were given. Subsequently, Zhang and Yu [8] promoted the application of steel-sheathed CFS shear wall in mid-rise construction by improving the shear capacities. The results showed that the use of blocking could effectively improve the shear strength of steel-sheathed shear wall. Similarly, Shi [9] developed two steel-sheathed CFS shear walls with higher shear resistance and stable mechanical behaviors for the same purpose.

Previous research has also proposed a CFS shear wall with corrugated steel sheathing as a lateral resisting system. As early as 2004, Fülöp [10] conducted shear tests on a series of CFS shear walls, the results of which indicated that damage to the corrugated steel sheathed wall was caused by screw damage at the panel seams. A cyclic loading test of corrugated steel sheathed wall specimens was conducted by Stojadinovic [11]. The author identified the recommended shear capacity of the corrugated steel sheathed shear wall under wind load and earthquake load. The three performance parameters of seismic design were also discussed. Waiel [12] compared the failure modes of corrugated steel sheathed shear walls with different thicknesses. A series of studies on shear walls with corrugated steel sheathing was undertaken at the University of North Texas. Yu et al. [13,14] found that the shear strength and stiffness of shear walls using corrugated steel sheathing were significantly improved compared with wood panel and flat steel plate sheathed shear walls. Yu et al. [15] and Zhang et al. [16] conducted further experimental studies on shear walls with corrugated steel sheathing. The results indicated that with a proper slit pattern, the corrugated steel sheathed shear walls exhibited significantly improved post-peak ductility and maintained a high level of shear resistance.

The previous studies show that the corrugated steel sheathed shear wall possesses high shear capacity and stiffness. Moreover, shear walls with corrugated steel sheathing are all-steel structures, which satisfy the non-combustibility requirement in IBC [17], and therefore could be used in mid-and high-rise CFS structures. However, all relevant research is limited to the component level. When involving the entire building, the connection between the floors, the ductility performance of the building, and the collapse-resisting capacity exhibited by the walls under strong earthquake action are all issues needed to be considered.

The shake table test is one of the common approaches by researchers to examine the seismic performance of buildings. The earliest shaking table tests of single-room house models with different structural configurations were conducted by Gad et al. at the University of Melbourne [18–20]. They concluded that the energy dissipation performance of a structure in the elastic-plastic stage could be improved by attaching a sheathing gypsum board on the inner side of the wall. The focus of research on later are primarily seismic performance of multi-story CFS structures. For instance, Dubina D [21,22] investigated the seismic performance of a two-story CFS structure in three stages by performing shaking table tests. The analysis showed that the sheathing plate plays a significant role in the energy dissipation and damping of the structure. Fiorino [23] divided the shaking table test of a two-story CFS house into two stages. The test results showed that the installation of nonstructural members in CFS structures can significantly increase the lateral building resistance. Moreover, unexpected and undesirable brittle failure modes could suddenly appear. Peterman and Schafer [24–27] conducted shaker tests on two double-story CFS houses. The main difference between the two models was whether the structure contained sheathing panels. The test results of both models proved that the CFS structure houses exhibited good seismic performance. Kim [28] performed a shaking table test on a full-scale two-story CFS structure. Lateral bracing of the model was provided by cross-bracing using thin tension-only straps in selected bays. The results indicated that during the large amplitude tests, the cross-bracing straps displayed very ductile but highly pinched hysteresis behavior. Shaking table tests of two reduced-scaled three-story models were undertaken by Fiorino et al. [29]. The walls of the two models were supported by cross bracing straps. However, unlike the model by Kim [28], strap braced walls were designed as non-energy-dispersing systems. The authors demonstrated that seismic response of strap braced CFS structure was satisfactory. Li et al. [30] conducted three full-scale shaking table tests on CFS structures, with the main differences between the models being the frame material strength and the sheathing material category. It's concluded that the structure had good seismic behavior and could be used in areas with high seismic intensity level. The unidirectional input shaking table test of five -and six-story CFS structures was carried out by Ye [31] and Wang [32], respectively. They also found that high-rise CFS structures exhibited good seismic performance, although bi-directional earthquake wave excitation was not adopted in their research.

In summary, few research has been conducted with regard to CFS buildings with corrugated steel sheathing. Besides, the limited research of CFS buildings has focused on the performance of overall structures under maximum design earthquakes. Moreover, the current seismic design codes [17,33–35] for structures involve the highest precautionary criterion as the risk-targeted maximum considered earthquake (MCE_R), with a 50a exceedance probability of 2%. However, the performance of the CFS structure under extremely rare earthquakes is also an important aspect of seismic and collapse-resistant design. Numerous high-intensity earthquakes have been encountered on a global scale in recent years, and actual regional seismic intensities are much higher than the precautionary intensities, indicating the possibility of extremely rare earthquakes. The concept of four levels of seismic action was first introduced in Chinese code GB50010-2010 [36], which added the extremely rare precautionary intensity with a 50a exceedance probability of 0.01%. Therefore, it is necessary to investigate the seismic performance of CFS structures under extremely rare earthquake.

This paper aims to increase knowledge of the seismic performance of corrugated steel sheathed CFS structures under extremely rare earthquake. A shaking test of a full-scale two-story CFS building with corrugated steel sheathing was conducted to investigate the dynamic behavior of the structure. Three seismic precautionary intensities and four precautionary criteria were considered in the test, including the conventional loading condition, and the extremely rare loading condition. The test program, observed phenomenon, and the analysis of the results are presented. Moreover, a simplified analytical model of the CFS building was simulated using OpenSees software and the seismic performance parameters of the CFS structure were discussed in order to aid the design process.

2. Shake table tests

2.1. Specimen configuration and design

A full-scale two-story CFS house model was designed to explore the dynamic properties and seismic response of CFS structures under extremely rare earthquake loads. Corrugated steel sheathing shear walls were used as the main seismic force-resisting system of these structures. The plane dimensions of the model were 2.8 m × 2.4 m, with an overall height of 5.693 m, as depicted in Fig. 1. This CFS structural model is designated in Chaoyang District, Beijing, China and has a seismic precautionary intensity of 8°, a design basic acceleration ground motion of 0.20g – the second seismic grouping – and a site classification of Class II. Therefore, the maximum value of the horizontal seismic influence coefficient of structure was 0.16, and the design characteristic period of ground motion was 0.4s. Seismic response modification factor (R) and structural over strength factor (Ω_0) are two main seismic design parameters of CFS structures. Both parameters of the CFS house model were designed with reference to the provisions of ASCE 7-16 [33], with R and Ω_0 taken as 6.5 and 3.0 respectively. The reasonableness of the identified seismic design parameters will be further verified in a later section.

Fig. 2 shows the plan layout of the CFS structural model. In addition to the three wall numbers (L1, L2 and L3), the drawing described the dimensions of the door and window openings and their positioning. The studs at the end and opening of the wall adopted the combined section forms I and II (made up of multiple C-shaped steel), respectively, while the other studs consisted of a single C-shaped steel part; the tracks, cross braces, and lintels of the wall were in the form of P-shaped steel. Detail of the shear walls are shown in Fig. 3. The connection details of the vertical and the horizontal walls are illustrated in Fig. 4. Strip connection fittings of 20mm × 60mm × 1 mm were used for the connection between walls with a spacing of 300 mm in the vertical direction. The connection fittings were mainly located on the inside and outside of the corners of the walls. The floor beams at the edge and opening adopted the composite section forms III and II, respectively, while the other floor beams consisted of a single C-shaped steel part. The connection details between the walls and the floor are shown in Fig. 5. The high-strength bolt of M16 ran through two hold-downs to fix the upper and the lower walls and the floor together on the inside of the structure. Meanwhile, Strip connection fittings of 70mm × 340mm × 1 mm were used for the connection of the wall and floor on the outside of the structure. The upper and lower chord members of the roof trusses were made of U-shaped steel, and the webs and roof panel braces were made of C-shaped steel. The roof was attached to the second-storey wall by six ST4.8 self-tapping screws at the point where the lower chord was in contact with the studs. The connection details between the walls and the roof are shown in Fig. 6.

The outer panel of the wall comprised a corrugated steel plate with a rib height of 5 mm and wave distance of 70.5 mm, while the inner panel was 12 mm thick gypsum board. The roof panel was made of corrugated steel with a rib height of 35 mm and wave distance of 125 mm. To reflect the light weight of CFS structures, an OSB was adopted for floor panels. The detailed sectional dimensions of the main components mentioned above are summarized in Table 1. The three material section shapes are listed in Table 1, and schematic diagrams of these are presented in Fig. 7. Table 2 and Fig. 8 depict the detailed layout of the three combined sections mentioned above. To ensure the CFS houses were firmly connected with the shake table, the model base was welded with hot-rolled section steel. The lower wall track was connected with the base through M16 shear bolts, and the model base was connected with the shaking table through M30 high-strength bolts. The assemble process of CFS structure model is shown in Fig. 9.

2.2. Material properties

The CFS members with different section forms used in the test model came from the same batch of steel; thus, their material

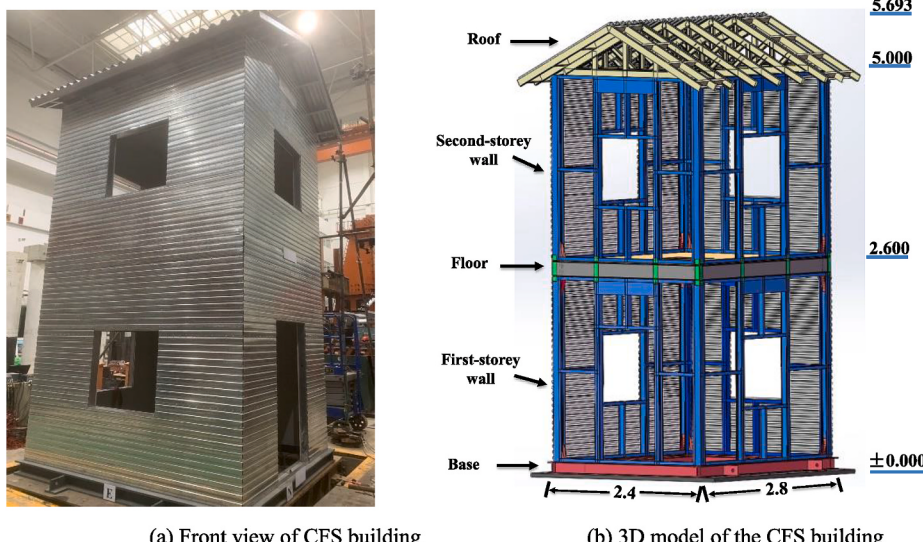


Fig. 1. Corrugated steel sheathed CFS structure model.

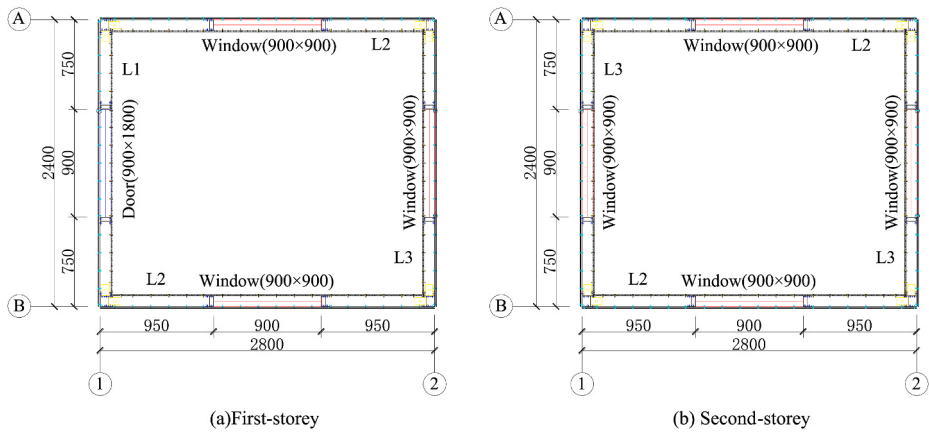


Fig. 2. Plan layout of the CFS structure model.

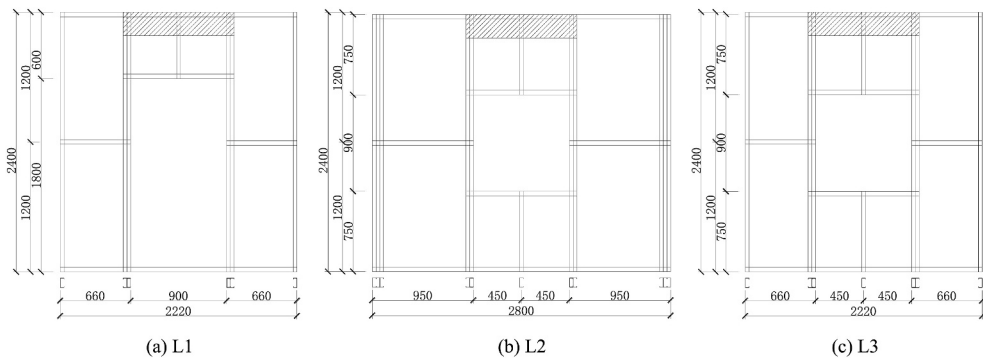


Fig. 3. Details of the shear walls.

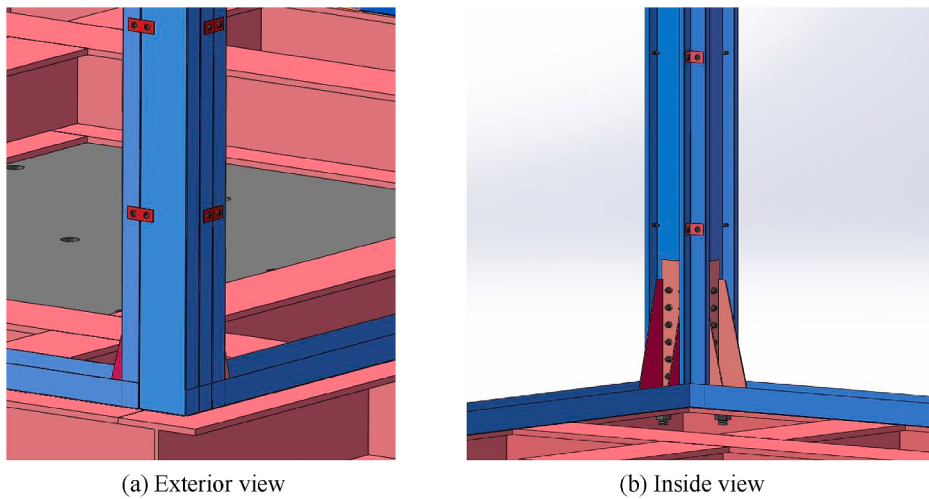


Fig. 4. Connection details of the vertical and the horizontal walls.

properties were the same. The material property test of the steel was based on Chinese Standard GB/T 228.1–2010 [37]. The aluminum-zinc coating was removed before standard material performance testing. The measured yield strength f_y of the steel was 375.96 MPa, tensile strength f_u was 456.57 MPa, elongation was 21.9%, and Poisson's ratio was 0.3. The tensile strength to yield strength ratios (f_u/f_y) exceeded 1.13, and elongations were greater than 10%, which satisfied the requirements of Chinese Standard GB/T 228.1–2010 [37].

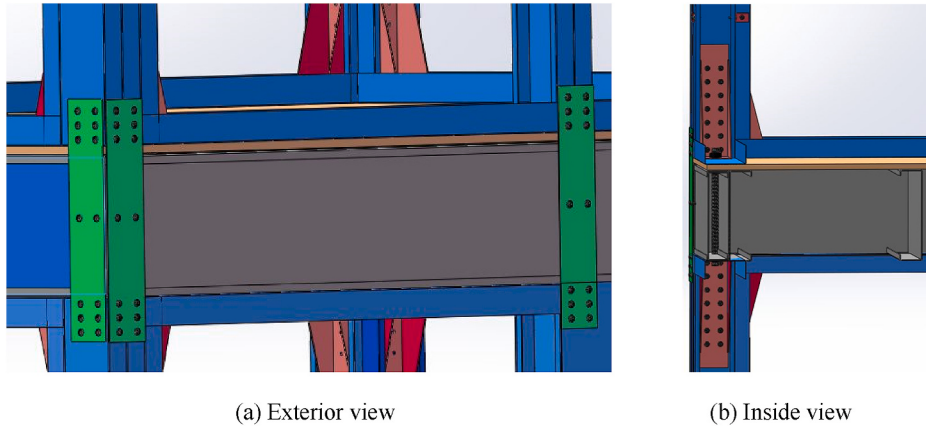


Fig. 5. Connection details between the walls and the floor.

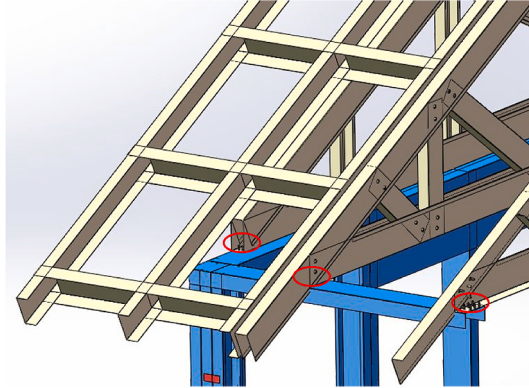


Fig. 6. Connection details between the walls and the roof.

Table 1

Dimensions of the main components of the structure.

Component element	Section shape	Section type	h/mm	b/mm	d/mm	t/mm
Stud-1, Roof panel brace	C-shaped steel	C9012	90	35	11	1.2
Stud-2		C8612	86	31	11	1.2
Floor beam-1		C20019	200	50	13	2.0
Floor beam-2		C19519	195	45	13	2.0
Web member of roof truss		C7012	70	35	11	1.2
Track, Cross brace	P-shaped steel	P9012	92	42	—	1.2
Floor side beam		P20019	204	56	—	2.0
Roof truss chord	U-shaped steel	U9012	90	40	11.5	1.2

2.3. Instrumentation

The shake table test was arranged with both acceleration sensors and displacement sensors. To obtain the actual acceleration value of the output at different positions of the CFS structure, acceleration sensors were arranged at the base of the model, the first floor, the second floor, and the roof. The detailed arrangement of the acceleration sensors is depicted in Fig. 10. Because the earthquake waves used in the test were input in both horizontal directions, displacement sensors were arranged in each of the two directions of the house model. The arrangement principle of the two types of sensors was basically similar, except for the top of the roof frame. The detailed arrangement of the displacement sensors is displayed in Fig. 11. There were 14 acceleration sensors and 8 displacement sensors in total. Sensor naming rules: A and D indicated the acceleration sensors and displacement sensors, respectively. The first number indicated the number of the story where the sensor was located; X and Y indicated the direction of sensor measurement; and the second number indicated the sensor number.

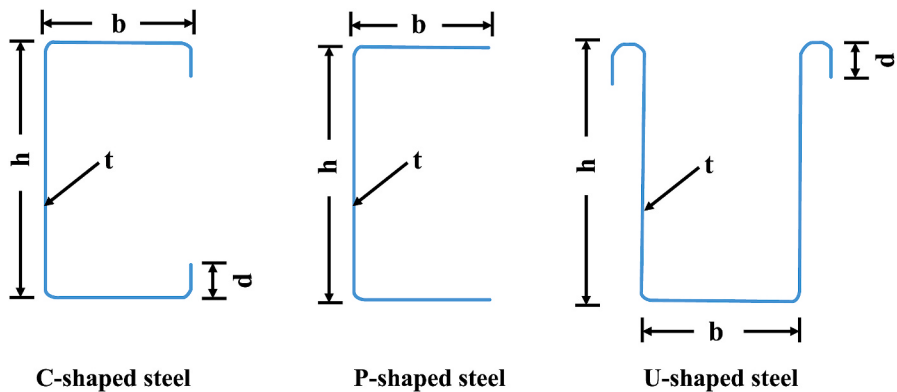


Fig. 7. Schematic diagram of section shape.

Table 2
Special combined section of components.

Structural element	Component element	Section type
Wall	Stud (ends)	Combined section I (C9012+C9012+C9012)
	Stud (openings)	Combined section II (C9012+C8612)
Floor	Beam (sides)	Combined section III (C20019+C19519+C20019)
	Beam (openings)	Combined section II (C20019+C19519)

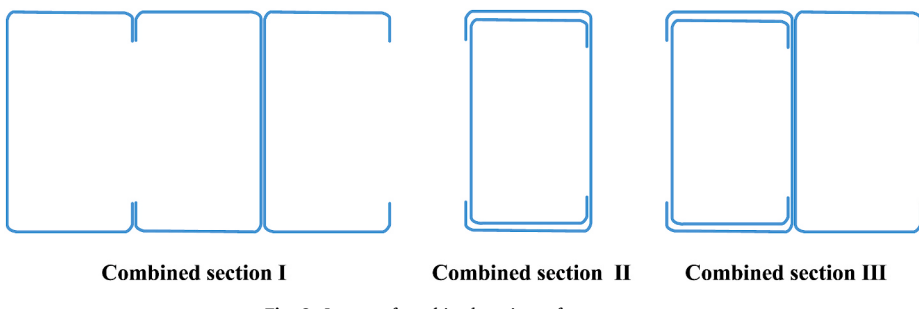


Fig. 8. Layout of combined sections of components.

2.4. Ground motion

The Chinese Standard GB50011-2001 [34] stipulates that when the time history method is adopted, no fewer than two groups of actual earthquake records and one group of artificially simulated acceleration time history curves should be selected according to the building site classification and design earthquake grouping. Therefore, three measured earthquake records (Lucerne wave, Santa Felita Dam wave, and Tangshan wave) and one artificial wave were selected for the test. To simulate earthquake action more accurately, the earthquake wave excitation input in this model was bidirectional. Thus, each earthquake wave was divided into two directions (eight seismic waves in total). The maximum displacement limit of the shake table was 100 mm, which meant the small frequency bands in all earthquake waves were filtered, reducing the horizontal displacement of the shake table. Finally, the frequency band of seismic wave was determined to be between 1Hz and 50Hz, and the frequency band outside the range was vastly different from the natural frequency of the CFS structure. This resulted in a negligible effect of filtering on the seismic response of the structure. The actual response spectra of filtered earthquake waves compared with the design response spectra is presented in Fig. 12.

2.5. Test procedure

In accordance with Chinese standard GB50009-2012 [38], the live load of residential floor was taken as 2.0 kN/m². Specification GB50011-2001 [34] stipulates that when calculating the seismic action, the combined value coefficient of the floor live load should be 0.5. In addition, the dead load increased by 0.20 kN/m² after the floor renovation. Finally, the counterweight applied to the first floor was 1.2 kN/m². The specification GB50011-2001 [34] adopted three precautionary criteria: frequent, moderate, and rare earthquakes. The North American Code IBC 2018 [17] is divided into two precautionary criterions with the same maximum precautionary criterions as the rare earthquake level. The maximum precautionary criterion in Eurocode EN 1998-1 [35] is the same as the moderate earthquake level. The actual situation regarding large earthquakes in the world in recent years, where the actual intensity of the earthquake zone is much larger than the precautionary intensity, highlighted the necessity of considering extremely rare earthquake



Fig. 9. Assemble process of the CFS structure model.

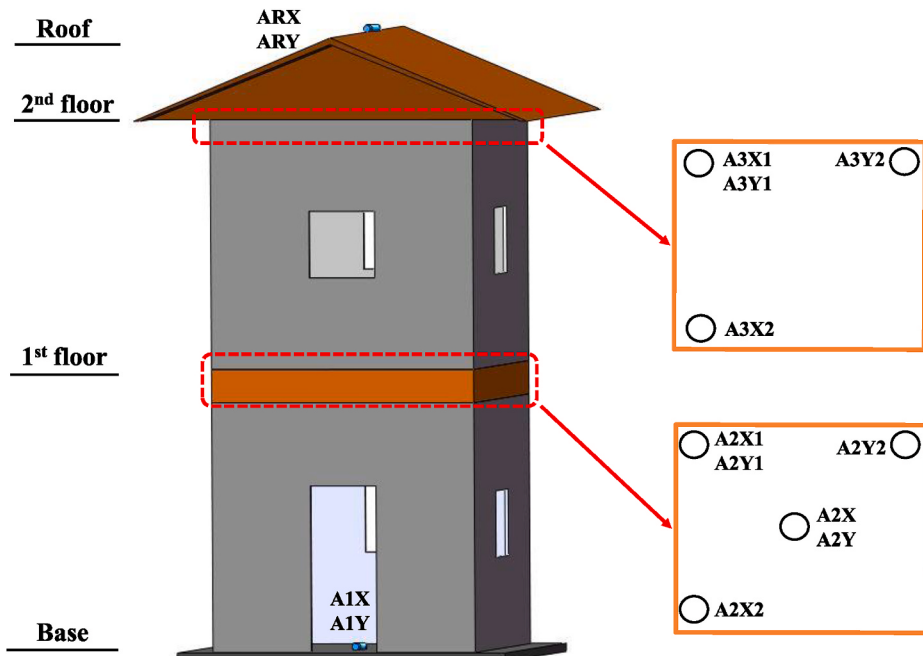


Fig. 10. Arrangement of acceleration sensors.

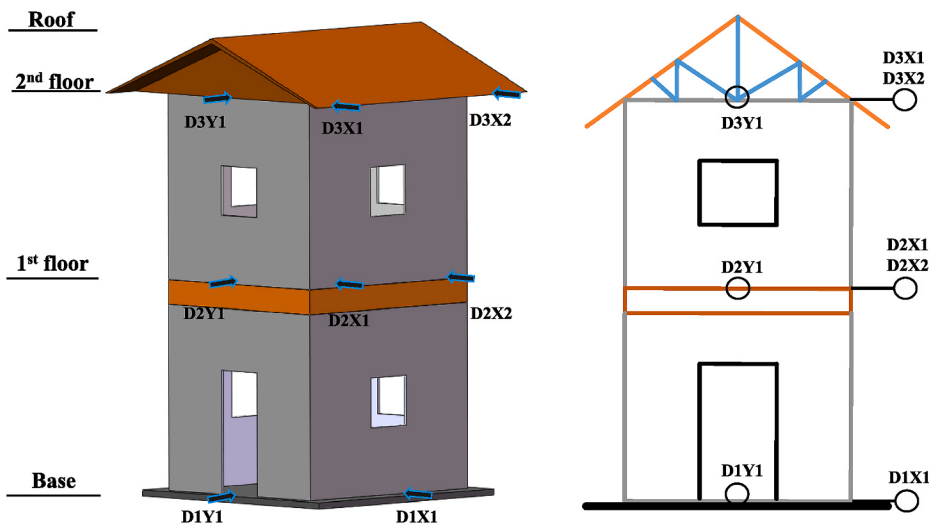


Fig. 11. Arrangement of laser displacement sensors.

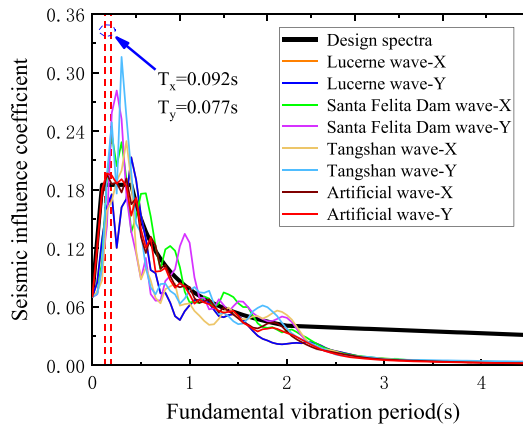


Fig. 12. Design spectra versus filtered seismic wave.

intensity in the seismic protection of structures. Three seismic precautionary intensities and four precautionary criterions were considered in this shake table test, the corresponding peak ground acceleration (PGA) of which are presented in Table 3.

The working conditions started from 0.035g and ended at 1.2g in the order of the PGA from small to large. When the PGA of the working conditions were the same or close to each other, only one would be taken. The working condition was divided into two stages. Stage I was the conventional loading condition, loaded from 0.035g up to 0.62g according to the PGA in Table 3. Stage II was the extremely rare loading condition, starting from 0.8g until 1.2g graded loading, where each level was loaded with 0.2g. The earthquake

Table 3
Maximum value of acceleration time history.

Precautionary intensity	Precautionary criterion	PGA (g)
7-degree	Frequent	0.035
	Moderate	0.1
	Rare	0.22
	Extremely rare	0.3
8-degree	Frequent	0.07
	Moderate	0.2
	Rare	0.4
	Extremely rare	0.6
9-degree	Frequent	0.14
	Moderate	0.4
	Rare	0.62
	Extremely rare	1.2

wave excitation input for this test was bidirectional, and the difference between the PGA in the main and secondary vibration directions was 0.85 times. After each working condition, the structure was swept by white noise. There were 100 working conditions in total. The test loading conditions are reported in Table 4.

3. Test phenomenon

The self-weight of the CFS structural house was lighter, so the house model could barely be observed significant vibration and displacement in the test loading pre-work condition (before working condition 45). When the PGA reached 0.22g, the seismic response of the structure could be observed in the building model. Particularly at the end of the rare earthquake condition (PGA of 0.62g), The damage of CFS structure began to occur in the inner panels of the walls and the floor panels, the failure phenomenon of which is shown in Fig. 13. As the seismic intensity increased, the damage degree of the CFS structure increased further. Up to the final loading condition (PGA of 1.20g), the damage of the building structure primarily occurred in the connections of screws and the inner panels. Fig. 14 and Fig. 15 depict the failure phenomenon of the CFS structure in detail. There was no obvious damage to the corrugated steel plates of the walls and roofs. Under high intensity conditions, the corrugated steel plates on the walls showed slight elastic deformation during the vibration, but returned to their original state after the vibration stopped. At the same time, the main structural frame exhibited no significant damage. The above phenomenon indicates that the structure resists the horizontal earthquake load primarily due to the diaphragm effect of the walls. When high intensity earthquake loads were applied, local damage occurred in the weaker wall panels of the structure. This weakened the diaphragm effect and thus led to a decrease in the seismic capability of the structural model.

Under the random reciprocal action of seismic loads, self-tapping screws appeared to tilt and slide, or sink to drill into and pull out of the gypsum board. The connection failure modes of screws are described in Fig. 14a-c. The main reason for failure was that in the case of high intensity, inertial forces were generated between the self-tapping screws and the gypsum board; this overcame their connection, resulting in relative slippage. Moreover, gypsum board was a brittle material, and when the house was shaken under earthquake load, the compression of screws on the gypsum board caused a certain degree of damage.

The damage to the panel mainly occurred on the gypsum board at the corner of the door frame and window, and the splicing seams position of the wall panel and roof panel. The failure modes of the panels are presented in Fig. 15a-f. The location of the window and door openings had a negative impact on the structure, and the panels were prone to stress concentration at the corner locations, causing cracks in the panels. Under high intensity conditions, the wallboards were extruded by the floor panels during structural vibration, while the gypsum board was a brittle material with local cracks. Similar to the above phenomenon, the wallboard and roof panel displayed extrusion damage. At the same time, the gypsum board exhibited dislocation under the action of self-weight.

4. Test results and analyses

4.1. Dynamic properties

The dynamic properties of the building structure reflect its inherent dynamic performance, which mainly includes basic parameters

Table 4
Loading conditions of the shaking table test.

Working condition type	Working condition number	Excitation wave type	Main vibration direction	PGA (g)	
				X	Y
White noise sweep	1/10/19/28 37/46/55/64 73/82/91/100	A	-	0.100	0.100
I: Normal loading condition	2/4/6/8 3/5/7/9 11/13/15/17 12/14/16/18 20/22/24/26 21/23/25/27 29/31/33/35 30/32/34/36 38/40/42/44 39/41/43/45 47/49/51/53 48/50/52/54 56/58/60/62 57/59/61/63 65/67/69/71 66/68/70/72	B	X Y X Y X Y X Y X Y X Y X Y X Y X Y	0.035 0.030 0.070 0.060 0.100 0.085 0.085 0.119 0.200 0.170 0.220 0.187 0.400 0.340 0.620 0.527 0.800 0.680 1.000 0.850 1.200 1.020	0.030 0.035 0.060 0.070 0.085 0.100 0.119 0.140 0.170 0.200 0.220 0.220 0.340 0.400 0.527 0.620 0.680 0.800 0.850 1.00 1.020
II: Extremely rare loading condition	74/76/78/80 75/77/79/81 83/85/87/89 84/86/88/90 92/94/96/98 93/95/97/99	B	X Y X Y X Y	0.800 0.680 1.000 0.850 1.200 1.020	0.680 0.800 0.850 1.00 1.020 1.200

The types of excitation waves were divided into A and B. A: White noise signal; B: Lucerne wave, Santa Felita Dam wave, Tangshan wave, artificial wave.

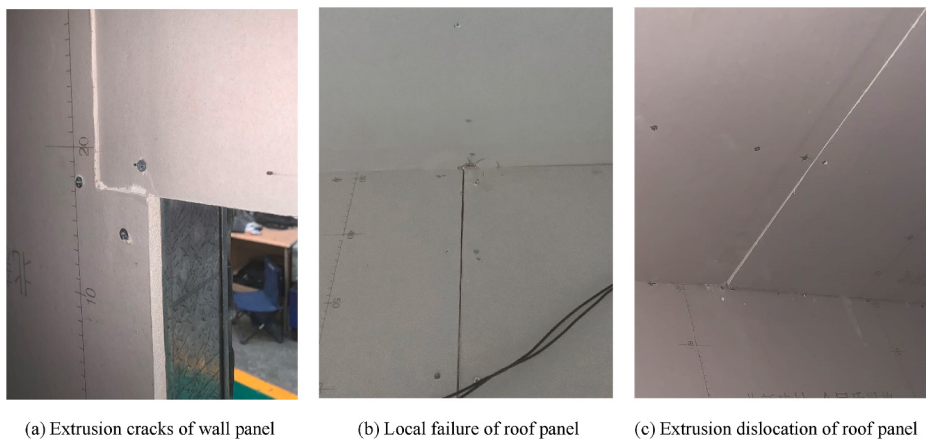


Fig. 13. Failure modes of CFS structure (PGA = 0.60g).

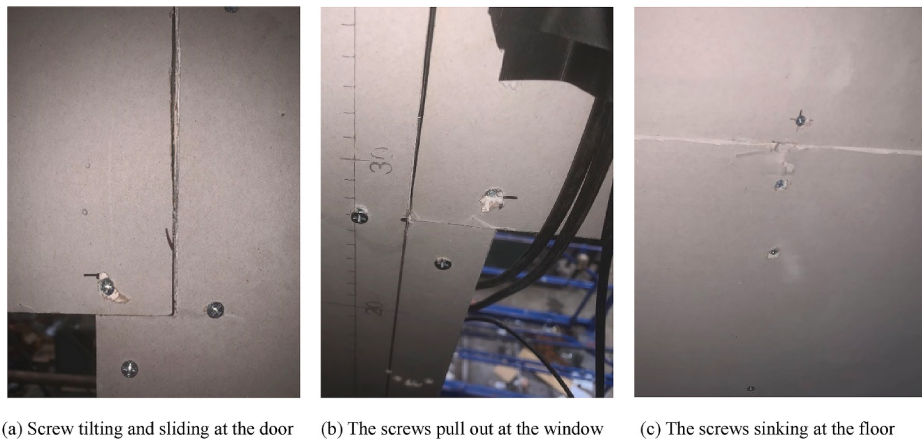


Fig. 14. Connection failure modes of screws (PGA = 1.20g).

such as natural frequency, stiffness, and the damping ratio of the structure. The transfer function curve of the model was obtained according to the acceleration time history of the shake table excitation in the white noise test and the acceleration response time history of the model. White noise sweeps were performed on the model structure before the start of the test and at the end of each working condition. Then, using transfer function curves, multiple dynamic parameters of the model structure were obtained to understand the variation in structural dynamic properties. Table 5 presents the results of the white noise test of the model structure.

4.1.1. Fundamental period and natural frequency

The natural frequency and fundamental period of the structure are its inherent properties, and are reciprocal to each other. As can be seen from Table 5, the initial natural frequencies of the structure in the X and Y directions were 10.89 Hz and 12.98 Hz, corresponding to periods of 0.092s and 0.077s, respectively. The natural frequency of the structure in the X-direction was smaller than that in the Y-direction, indicating that the stiffness of the structure in the X-direction was relatively weak. The main reason for this was that the effective width of the wall in the X direction of the model structure was less than that in the Y direction. This is also consistent with the fact that the seismic response of the structure in the X direction was greater than that in the Y direction.

Fig. 16 depicts the trends in variation of the natural frequency and fundamental period. As the seismic intensity increased, the natural frequency decreased and the fundamental period increased in both directions of the structure. The trend of natural frequency and fundamental period was minimal until the white noise condition was 46; in subsequent working conditions, the magnitude of the variation between the two started to increase gradually. Most notably, after the white noise condition sweep was 73 (9-degree rare condition), the change rate of the two reached their peak, after which the change rate remained unchanged until the end of the extremely rare condition. This indicated that greater damage to the structure began to occur after the 9-degree rare condition. As seismic intensity increased further, the accumulation of damage led to a decrease in stiffness and a greater rate of change in the natural frequency and fundamental period of the structure.

4.1.2. Damping ratio

Damping is one of the most important parameters in the analysis of structural dynamic properties. It reflects the ability of structural



Fig. 15. Failure modes of panels (PGA = 1.20g).

Table 5
Frequencies and damping ratios of the test model.

White noise condition	X-direction			Y-direction		
	Frequency (Hz)	Period (s)	Damping ratio (%)	Frequency (Hz)	Period (s)	Damping ratio (%)
1	10.89	0.092	2.59	12.98	0.077	2.23
10	10.77	0.093	2.43	12.88	0.078	1.95
19	10.68	0.094	2.22	12.82	0.078	2.5
28	10.65	0.094	2.65	12.90	0.078	2.55
37	10.53	0.094	2.92	12.84	0.078	2.59
46	10.50	0.095	3.04	12.80	0.078	2.28
55	10.18	0.098	3.34	12.67	0.079	3.44
64	10.01	0.099	3.78	12.65	0.079	3.93
73	9.54	0.106	4.66	12.30	0.082	4.12
82	9.08	0.110	5.98	11.97	0.084	6.08
91	8.08	0.124	7.37	11.24	0.089	6.66
100	7.11	0.141	7.52	10.70	0.094	6.77

energy dissipation; the greater the damping, the stronger the energy dissipation performance of the structural model. The model damping ratio variation curves are presented in Fig. 17. As the load intensity increased, the damping ratio of the structure increased. As with the fundamental period variation, the damping ratio of the structure grew further and the energy dissipation capacity of its structure increased under the action of a high-intensity earthquake.

Before the white noise condition was 55, the damping ratio of the structure was 2%–3%, which was consistent with the provisions of Chinese specification JGJ 227–2011 [33]: the damping ratio of CFS structures was taken as 3% when calculating the horizontal seismic action. When the white noise condition was 55, the damping ratio exceeded 3%. When the white noise condition was 73

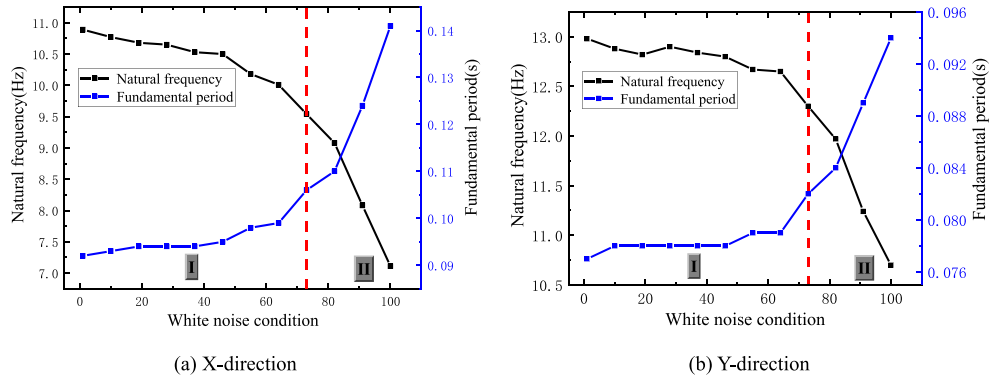


Fig. 16. Variation curve of natural frequency and fundamental period.

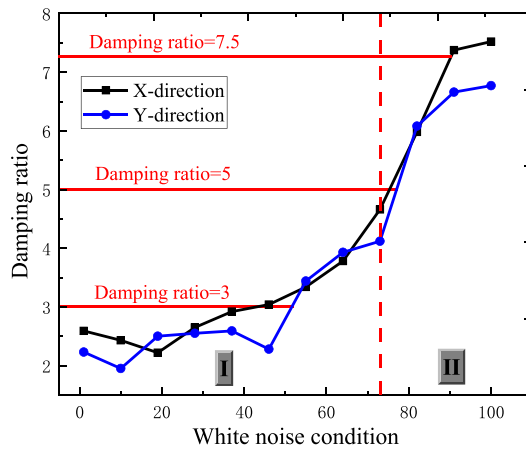


Fig. 17. Variation curve of damping ratio.

(9-degree rare condition), the damping ratio of the structure was close to 5%, which was the same as the damping ratio taken for other common building structures [28]. When the white noise condition was 100, i.e., the earthquake intensity reached 9-degree extremely rare, the maximum structural damping ratio reached 7.52% in the final white noise condition. This indicated that under ultra-high seismic intensities, the house structure already had significant internal damage and increased its energy dissipation capacity to resist the seismic loads. This needs to be taken into account in seismic design as well as in numerical simulations. Finally, it is suggested that the damping ratio of the structure in the nonlinear phase should be in the range 5%–7.5% given the degree of structural damage.

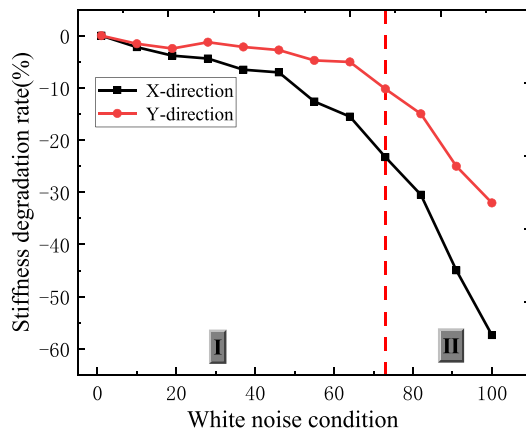


Fig. 18. Variation curve of stiffness degradation.

4.1.3. Stiffness degradation

The stiffness of the structure is proportional to the square of the natural frequency while keeping the model mass constant. Therefore, the change in stiffness of the structural model is expressed by the change in its natural frequency. The stiffness degradation rate (*SDR*) of CFS structural was obtained as follows:

$$SDR = \frac{k_1 - k_0}{k_0} = \frac{f_1^2 - f_0^2}{f_0^2} \quad (1)$$

where k_1 , k_0 are the stiffness of the structure during the test and the initial stiffness before the test, respectively; and f_1 , f_0 are the natural frequencies corresponding to k_1 , k_0 .

Fig. 18 depicts the trend in the *SDR* of the structure after each working condition of the model. The *SDR* of the structural model increased in line with earthquake load intensity, but the attenuation trend in both directions was not consistent, and its stiffness attenuation amplitude in the X-direction was greater than in the Y-direction. This difference also indicated that the X-direction of the structure was the weak stiffness direction, which is consistent with the theoretical analysis of the natural frequency, fundamental period, and damping ratio in the previous section. In the early stage of the normal loading condition, the stiffness degradation of the structure displayed a certain increase, which was mainly caused by the closure of the gaps at the seams of the members in the CFS structure. When the white noise condition was 55, the stiffness of the structure started to decrease. At the working condition of 73, the stiffness of the structure exhibited a significant decrease, and the *SDR* was nearly 25%. The stiffness of the structure continued to decrease at the same rate of change during the extremely rare loading condition phase, especially in the final condition (9-extremely rare condition), where the *SDR* was close to 60%. This was due to the obvious seismic response of the structure under the 7-rare earthquake load. In the subsequent working condition, the wall panels exhibited extrusion local damage, enlargement of the seams between the panels, and loss of self-tapping screws. At this point the diaphragm effect of the structural wall was weakened, resulting in degradation of the overall stiffness of the structure. Under the continuous action of earthquakes of rare and extremely rare intensities, structural damage accumulated and a substantial decrease in stiffness occurred. Although the above-mentioned damage and phenomena occurred in the final model of the house, ultimately there was no obvious damage to the frame of the structure. Consequently,

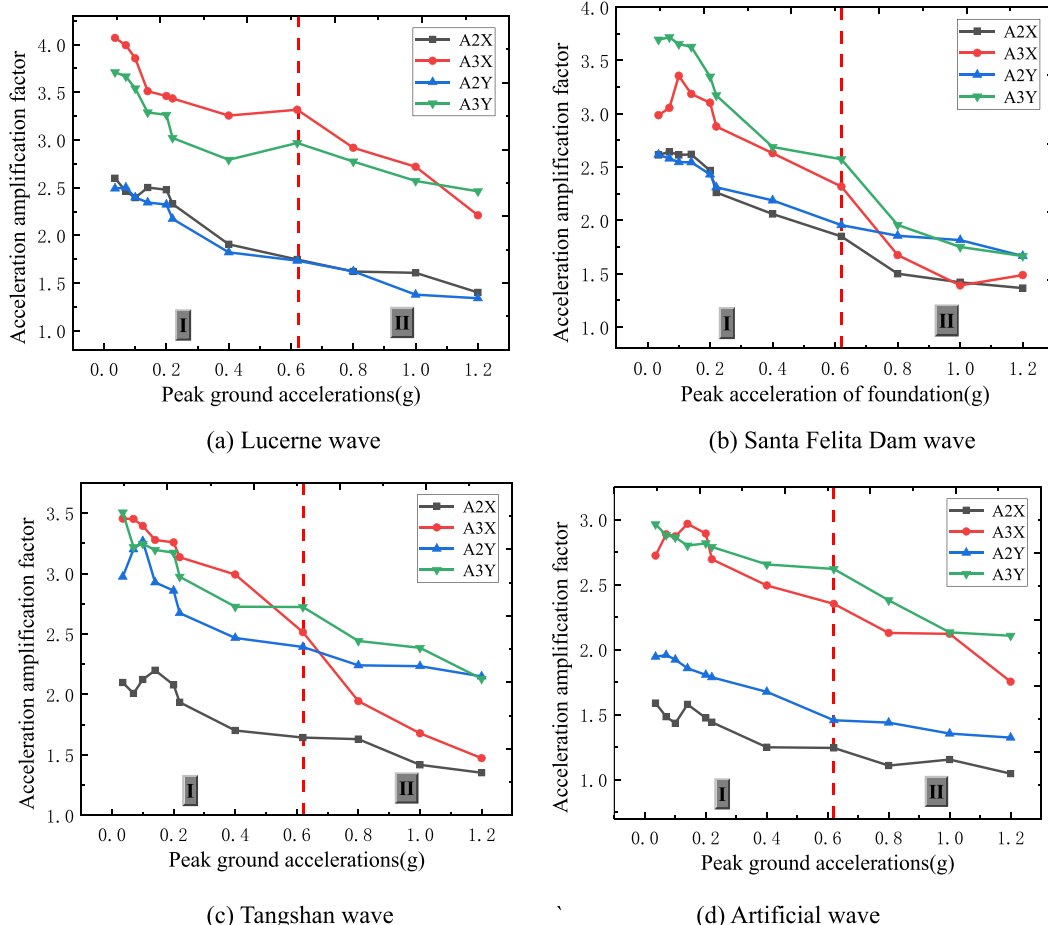


Fig. 19. Acceleration amplification factor of the structural model.

the CFS structural model did not appear to be in danger of collapse, which preliminarily indicates that the structural system meets the seismic design requirements for extremely rare conditions.

4.2. Seismic response

4.2.1. Acceleration response

The acceleration response of the structure is related to the characteristics of the actual response spectra, the natural frequency of the structure, and the damping ratio of the structure, which is an important parameter of the structural dynamic response. The absolute acceleration response of the model structure under each working condition was measured by the acceleration sensors set at each position of the model. The acceleration amplification factor (AAF) was calculated using the following equation:

$$AAF_i = \frac{\max|a_i|}{\max|a_{ST}|} \quad (2)$$

where a_i and AAF_i represent the absolute acceleration and acceleration amplification factor on the i -th story of the structure, respectively; and a_{ST} is the absolute acceleration of the shake table along the loading direction.

The trend in the acceleration amplification factors of the structural model is displayed in Fig. 19. The peak acceleration and amplification factor tended to increase in line with height. In the above analysis, the X-direction of the structure was the weak stiffness direction. However, in the same working condition, the acceleration response in the X-direction was not necessarily greater than that in the Y-direction. The reason for this was that the dynamic properties of CFS structures changed all the time under earthquake load, and the characteristics of actual response spectra in two directions were different. The AAF of the model gradually decreased as the PGA of the table excitation increased. This was due to the fact that as the ground motion intensity increased, the structural damage continued to accumulate, and the stiffness degradation and the fundamental period became longer, resulting in the continuous decrease of the AAF. In the early working condition of the first stage, the AAF fluctuated up and down in a small range, which was caused by closure of the gap at the connection of the structure under the action of earthquake load. At a PGA of 0.22g, there was a significant decrease in the acceleration amplification factor. When the second stage was entered, the acceleration amplification coefficient of the structure decreased further. Most notably, under the 9-degree extremely rare working condition (PGA of 1.2g), the maximum difference of AAF was 2.03 compared with the initial one. This also indicated that the structure experienced greater damage under extremely rare earthquake load, which is consistent with the results of the stiffness degradation analysis in the previous section.

Fig. 20 depicts the functional relationship between the acceleration amplification factor of the model and the structural height, where z is the height of the accelerometer arrangement location and h is the roof height of the CFS structural model. In EN 1998–1 [35] and ASCE 7–16 [33] a linear correlation exists between acceleration amplification factor and z/h . In the first stage, when z/h equaled 0.44 or 0.847 (position of first floor or second floor), the acceleration amplification factor for the artificial wave condition agreed well with ASCE 7–16 [33]; when z/h equaled 1 (roof position), the relationship given by EN1998-1 [35] and ASCE 7–16 [33] underestimated the variation in the AAF, equivalent to the results of Fiorino L [23]. However, the acceleration amplification factors (AAFs) for other seismic wave conditions in the first stage, except for artificial waves, differed significantly from the linear curves of specification. The distribution of the two was more scattered, and the relevant provisions of the specification were too conservative. This was because the AAF was mainly determined by the actual response spectra characteristics of the structure, as well as its fundamental period and damping ratio. The AAFs of the model under the action of different earthquake waves differed substantially, and their trends could not be expressed by a simple linear relationship. Due to the influence of the spectrum characteristics, the second stage was similar to the first stage, and only some of the data existed to match the specification. Therefore, the provisions of EN 1998–1 [35] and ASCE 7–16 [33] were too conservative to assess the seismic response of CFS structures with respect to acceleration amplification factors. In future research, the investigator should establish the function relationship of the acceleration amplification coefficient based on a large amount of experimental data, taking several influencing factors into account in a comprehensive manner.

4.2.2. Displacement response

Fig. 21 depicts the time history of floor horizontal displacement measured by representative sensors. The time history of CFS structure in the figure is mainly based on the displacement data in the representative working conditions of Lucerne wave. It should be noted that this floor displacement was relative with respect to the CFS structural model base. The floor horizontal displacement in the X-direction was an average value of two displacements measured at the edge of each side of the floor; the floor horizontal displacement in the Y-direction was the value measured in the middle of the floor. When the PGA reached 0.14g, the horizontal displacement of each floor of the structure was basically small, and increased approximately linearly with the building height. However, the degree of increase in the horizontal displacement of the first floor was higher than that of the second floor at higher intensities. The floor displacement response in the X-direction was relatively large compared with the Y-direction of the CFS structure. The CFS structure with a PGA of 0.14g behaved in an elastic manner, and in higher intensities it behaved in an inelastic manner, although most of the inelastic behavior was concentrated in the first story. This is mainly attributable to the greater inertial force of the first story under the earthquake load compared with the second story; thus, the first story of the CFS structure entered the plastic phase first, which can also be observed in the following story drift ratio analysis.

The inter-story drift ratio is an important indicator and basis for assessing the degree of structural damage from a macroscopic level. The absolute displacement data of the model structure under each working condition were measured by the displacement sensors set at each floor of the model. The peak inter-story drift ratio (PIDR) of CFS structural was obtained as follows:

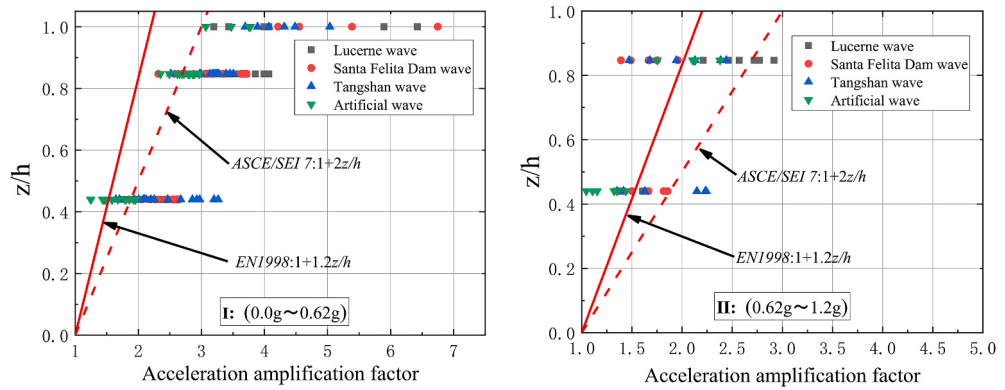
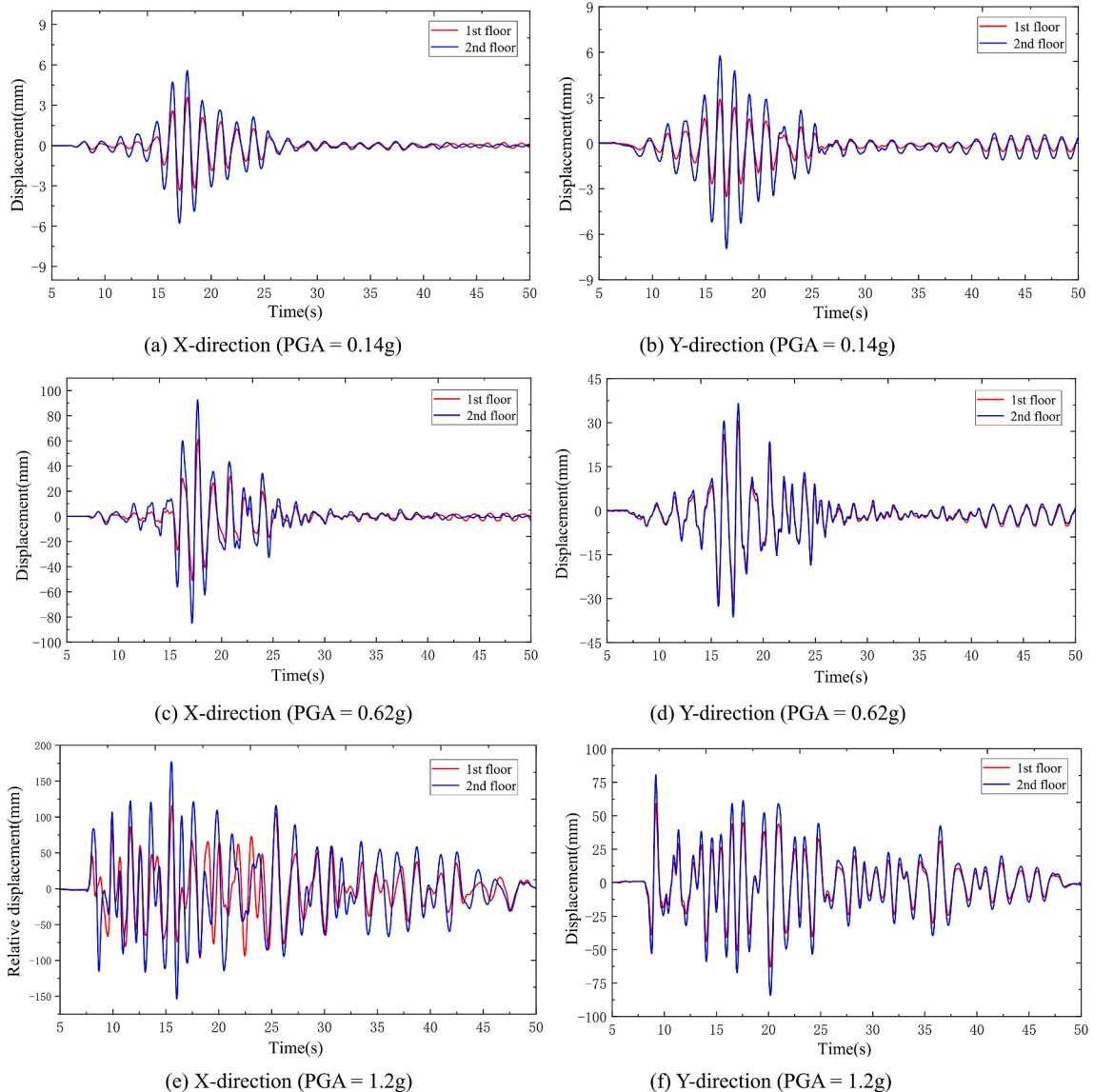
Fig. 20. Acceleration amplification factor versus z/h .

Fig. 21. Time history of floor horizontal displacement (Lucerne Wave).

$$PIDR_i = \frac{\max|d_{Li} - d_{ST}|}{h_i} \quad (3)$$

where h_i , d_i and $PIDR_i$ denote the floor height, absolute displacement, and peak inter-story drift ratio on the i -th story of the structure, respectively; and d_{ST} is the displacement of the shake table along the loading direction.

Table 6 lists the $PIDR$ at each position of the structural model for different operating conditions. θ_{1X} , θ_{2X} , θ_{1Y} and θ_{2Y} in the table represent the peak inter-story drift ratios of the first-storey and second-storey of the structure in their respective directions. In the same direction of the CFS structure, the peak inter-story drift ratios ($PIDRs$) of the first story were greater than those of the second story. This is because the self-weight of the second story wall and roof of the model was transmitted to the lower story of the structure, and all the counterweight of the model was added to the first floor. Therefore, the shear value of the first story wall of the structure was much greater than that of the second story wall under the action of an earthquake. On the premise that there was little difference in the stiffness of each story of the wall, its $PIDR$ was mainly determined by the shear value.

The comparisons of $PIDR$ between test and specification are plotted in **Fig. 22**. The $PIDR$ of the structure was 0.214% under the action of a 9-degree frequent earthquake (PGA of 0.14g). This satisfied the requirement of Chinese specification JGJ227-2011 [39] that the inter-story drift ratio of the structure under frequent earthquake action should be less than 1/300. The seismic specification JB50011-2001 [34] on the peak plastic inter-story drift ratio of high-rise steel structure should be less than 1/50, but its object of seismic specification was a high-rise steel structure, which is very different from the CFS structure. According to ASCE 7-16 [33], the allowable inter-story drift of a CFS structure under seismic load is 1/40 of the story height. The $PIDR$ was 2.329% under the action of a 9-degree rare earthquake (PGA of 0.62g). This exceeded the limit of 1/50 of the inter-story drift ratio of JB50011-2001 [34], but satisfied the relevant provisions of North American code ASCE 7-16 [33]. The FEMA P695 [40] recommends a limit of 7% for the collapse drift ratio of light wood-frame structures. At the same time, specification FEMA P695 [40] does not provide a recommended drift limit for CFS structures. However, the latter were similar to the structural system of light wood-frame structures. International building code [41] and ASCE 7-16 [33] assign the same seismic performance factors to both systems. Moreover, the literature [42,43] suggests that it is reasonable and conservative to use 7% as the collapse drift ratio limit for CFS structures. The $PIDR$ of first story was 4.405% under the action of a 9-degree extremely rare earthquake (PGA of 1.2g), far below the requirement of a collapse drift ratio limit. while the structure did not appear to be in danger of collapse during the test phenomenon. Although the first story of the CFS structures displayed nonlinear behavior, they did not appear to be in danger of collapse during the test. Therefore, corrugated steel sheathing CFS structure offers extremely good shear resistance and seismic performance which can meet the requirements of multi-level seismic precautions and provide a reference for the seismic design of the structure under extremely rare conditions.

5. Seismic design assessment

5.1. Finite element modeling

The nonlinear dynamic analysis software OpenSees was used in the finite element analysis. The data from the above shaking table tests were used to model the CFS structure. **Fig. 23** illustrates the schematic of the finite element model used in OpenSees. The modeling technique was in accordance with Zhang et al. [44]. To improve the computational efficiency of the model, the rigid floor assumptions were used to simulate the floor and roof system of CFS structure. A rigid diaphragm was used for the model by a built-in element in OpenSees. The total mass of the structure was calculated based on the design documentation of the test specimens, with the mass of each story evenly distributed over the four corners of each level. The weight was achieved by applying acceleration of gravity to the CFS structure.

The shear wall model was composed of two diagonal truss elements and elastic frame boundary elements. The diagonal truss elements used Pinching4 uniaxial hysteresis material from OpenSees to simulate the stiffness degradation, the pinching effect and the strength degradation, as shown in **Fig. 24**. The parameters involved in Pinching4 material model were based on CFS shear wall testing data from the Liu [45], listed in **Table 7**. The Pinching4 parameters of CFS shear wall was the key to modeling the CFS structure. To verify the validity of the shear wall model, the wall specimens using corrugated steel sheathing were simulated. The test result and the

Table 6
Peak inter-story drift ratio of the structural model.

Phase	Working condition	Measuring point	Peak inter-story drift ratio (%)			
			Lucerne wave	Santa Felita Dam wave	Tangshan wave	Artificial wave
I	9-degree frequent (0.14g)	θ_{1X}	0.137	0.147	0.210	0.147
		θ_{2X}	0.105	0.110	0.112	0.107
		θ_{1Y}	0.133	0.122	0.214	0.134
		θ_{2Y}	0.128	0.105	0.128	0.116
	9-degree rare (0.62g)	θ_{1X}	2.329	1.422	1.186	1.474
		θ_{2X}	1.186	1.129	1.045	1.329
		θ_{1Y}	1.211	1.529	1.025	1.43
		θ_{2Y}	0.210	0.233	0.175	0.198
II	9-degree extremely rare (1.2g)	θ_{1X}	4.405	3.002	2.283	3.085
		θ_{2X}	2.333	2.158	1.919	2.760
		θ_{1Y}	2.399	3.072	1.863	2.701
		θ_{2Y}	0.814	1.090	0.673	1.008

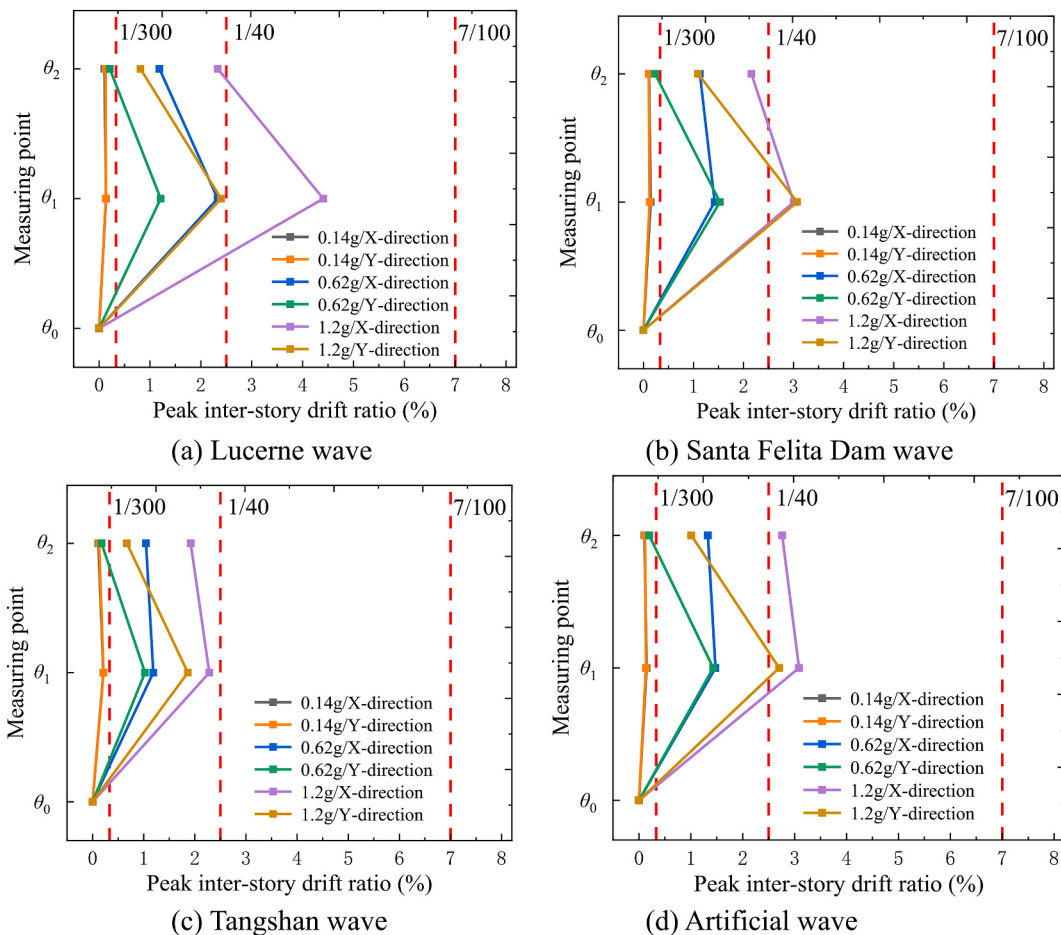


Fig. 22. Comparisons of peak inter-story drift ratio between test and specification.

finite element result are compared in Fig. 25. It could be seen that the finite element results of shear wall are in good agreement with the test results. The finite element model of the wall was able to reflect the hysteretic properties of the wall and to simulate the degradation process of strength and stiffness.

5.2. Verification of finite element models

According to the Chinese specification JGJ227-2011 [39], the bearing capacity of the double-sided wall can be taken as the sum of the respective bearing capacities of the individual panel wall (corrugated steel sheathed wall and gypsum board sheathed wall). Since the shear wall in Liu [45] was single-sided sheathed, it is necessary to modify the bearing capacity values of the numerical model according to Ref. [39]. The validity of the CFS structural model was verified by performing a non-linear dynamic time analysis on a model structure of the CFS house under typical conditions (PGA = 0.40g). The eigenvector method was used to the model, with periods of 0.095s and 0.076s in both directions of the structure, which were almost identical to the actual measured periods. The comparison of time history curve of the Tangshan and lucerne waves is shown in Fig. 26 and Fig. 27. The simulated peak accelerations and peak displacements were relatively close to the test results, with errors within 6%, and the shapes of the time history curves were in good agreement. Therefore, the computational accuracy of the simplified analytical model of the CFS structure was within an acceptable range and could simulate the dynamic response and seismic properties of the structure more accurately.

5.3. Response modification factor

The response modification factors were first introduced by the Applied Technology Council in ATC-3-06 [46] report. The core of the concept is that a well-designed structure has excellent displacement ductility and are able to carry large inelastic deformations without collapse. It is also important to ensure that damage to specific components could not affect the overall stability of the structure. Demand reduction from the elastic strength demand to real inelastic strength is taken into account using the reduction factors. The response modification factor is composed of both the ductility reduction factor (R_d) and the structural over strength factor(Ω_0) and defined as

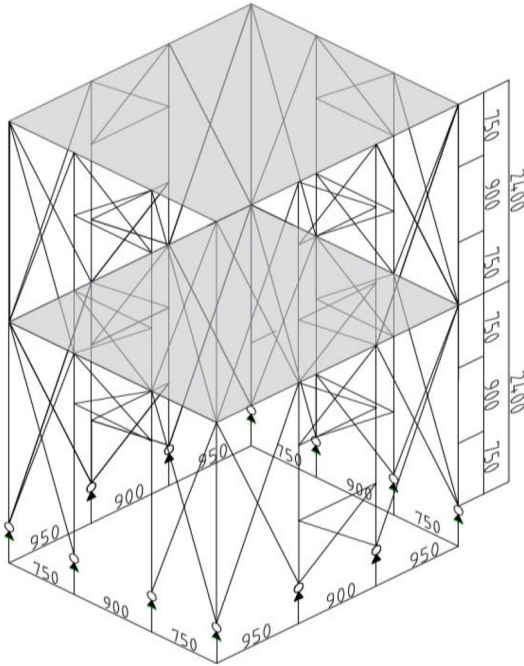


Fig. 23. Schematic model of CFS structure (unit: mm).

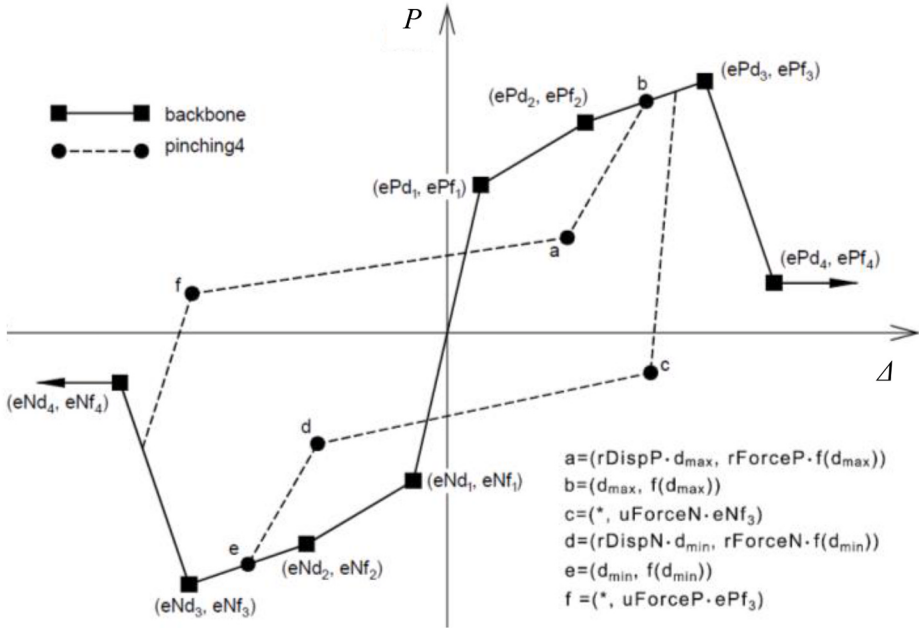


Fig. 24. Pinching4 material model.

$$R = R_d \times \Omega_0 = \frac{V_e}{V_y} \times \frac{V_y}{V_s} = \frac{V_e}{V_s} \quad (4)$$

Where V_e , V_s and V_y correspond to the structural elastic response strength, the first significant yield strength, and the idealized yield strength respectively, the meanings represented by these strength values are detailed in Fig. 28.

Fig. 28 mainly indicates the general structural response and the idealized response. The idealized bilinear curve is a force-displacement curve consisting of two lines based on ASCE 41-13 [47]. The line segments should be located using the iterative

Table 7
Pinching4 parameters of CFS shear wall.

Pinching4 parameters	Value	Pinching4 parameters	Value
ePd ₁ , eNd ₁	0.29	gKlim	0.90
ePd ₂ , eNd ₂	0.59	gD _{1,2}	0.40
ePd ₃ , eNd ₃	1.00	gD _{3,4}	2.00
ePd ₄ , eNd ₄	2.70	gDlim	0.50
ePf ₁ , eNf ₁	0.22	gF ₁	1.00
ePf ₂ , eNf ₂	0.76	gF ₂	0.00
ePf ₃ , eNf ₃	1.00	gF _{3,4}	1.00
ePf ₄ , eNf ₄	0.55	gFlim	0.90
gK ₁	-1.00	rForce	0.13
gK ₂	-0.20	uForce	-0.10
gK ₃	0.30	rDisp	0.10
gK ₄	0.20	gE	10.00

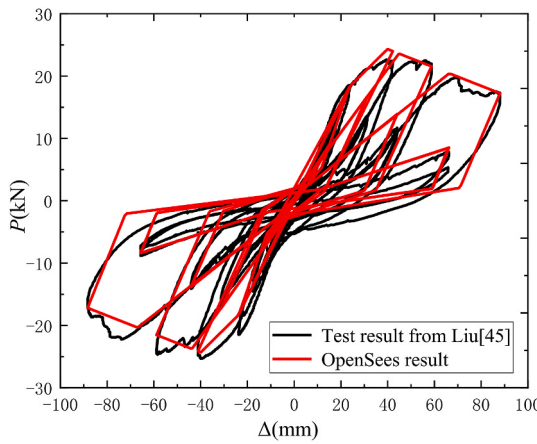


Fig. 25. Comparison of hysteresis curves of shear walls.

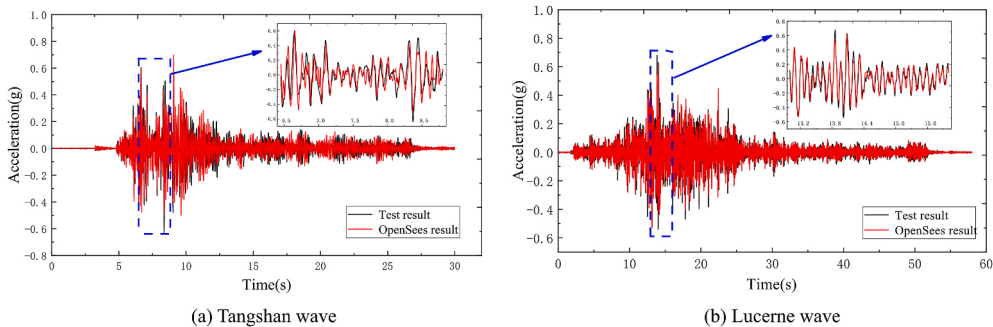


Fig. 26. Comparison of acceleration time history curve (PGA = 0.40g).

graphical method to balance the size of the areas of the idealized and actual curves. The initial secant stiffness of 60% of the idealized yield strength is shown by the slope of the first line segment. The second line segment shall be specified by a line passing through the actual curve at the calculated target displacement (Δ_t). The target displacement was determined to be the corresponding displacement when the structural strength was reduced to 80% of the peak strength in this study.

Newmark and Hall [48] developed an alternative method for calculating the ductility reduction factor, which has been widely adopted by other researchers. The method starts by obtaining the structural ductility $\mu = \Delta_t/\Delta_y$, and then the ductility reduction factor be determined in terms structural ductility as follows:

$$R_d = \mu T > 0.5s \quad (5)$$

$$R_d = \sqrt{2\mu - 1} \quad 0.1s < T < 0.5s \quad (6)$$

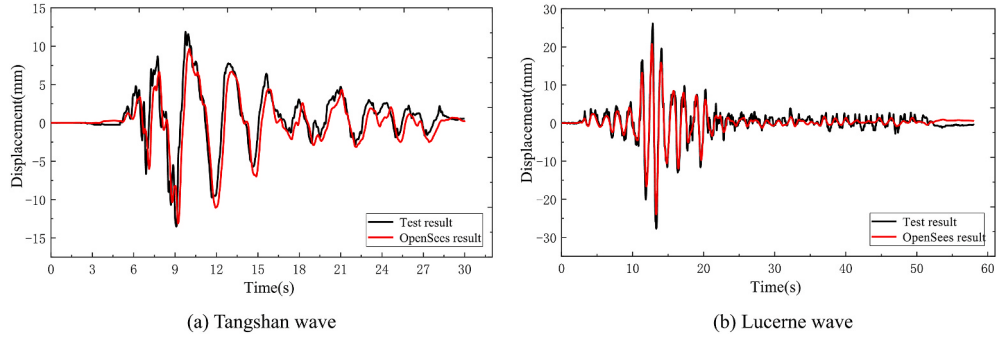


Fig. 27. Comparison of displacement time history curve (PGA = 0.40g).

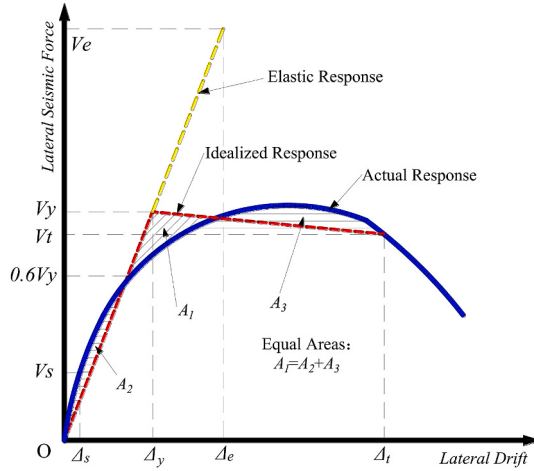


Fig. 28. General Structural response.

$$R_d = 1 \quad T < 0.03s \quad (7)$$

The first significant yield strength V_s can be evaluated using Fig. 29. The drift deviation between the envelope curve and the linear trend can be calculated using Eq. (8). When the significant yield point is a drift deviation of less than 0.5%, the corresponding lateral load can be derived and recorded as the first significant yield strength V_s .

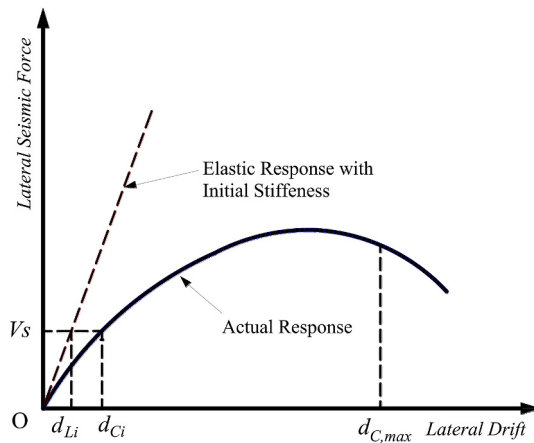


Fig. 29. Calculation of the drift deviation.

$$D_i = \frac{d_{Li} - d_{Ci}}{d_{C,max}} (\%) \quad (8)$$

Where D_i is the drift deviation associated with the i -th point; d_{Li} is the drift of the linear trend associated with i -th point; d_{Ci} is the drift of the envelope curve associated with i -th point; and $d_{C,max}$ is the maximum displacement of the shear wall.

Pushover analysis is currently used as a practical analysis method to evaluate the seismic performance of structures. In this paper the first formation distribution model recommended by FEMA P695 [40] is used to load the structure horizontally. The non-linear Pushover curve of a CFS structure is obtained by applying a monotonically increasing load to the structure and gradually bringing the structure to a specified target displacement. Fig. 30 shows the pushover curve of CFS structure. The response modification factors of CFS structure are listed in Table 8. The structural overstrength factor (Ω_0) and the response correction factor (R) were greater than 3.0 and 6.5 in both directions respectively, while the CFS structure performed well in the tests in terms of seismic performance. As a result, the adoption of the values specified in ASCE 7-16 [33] ($R = 6.5$ and $\Omega_0 = 3.0$) was confirmed for this newly proposed lateral resisting system with corrugated steel sheathing.

6. Conclusions

The paper presented the shake table test results of a full-scale two-story CFS structure, of which the seismic force-resisting system was provided by corrugated steel sheathed shear walls. In particular, the seismic performance of the CFS structural model under extremely rare earthquake loading conditions was evaluated in addition to the normal earthquake loading. The principal outcomes of the study can be summarized as follows:

1. Damage of the corrugated steel sheathed CFS structure began to occur in the walls and floors under rare earthquakes and increased further with the intensity of the earthquake. The final damage mainly took the form of connection damage to the screws and local damage of the inner panels, while the steel frame remained basically intact under extremely rare precautionary intensity.
2. Compared with the normal loading condition, the variation in the dynamic properties of the structure in the extremely rare loading condition phase increased further. In the seismic analysis of the CFS structure, it is recommended that the damping ratio of the structure in the nonlinear phase should be in the range of 5%–7.5%.
3. The AAF basically tended to increase with structural height, and its trend in the EN1998 and ASCE 7 was identified as a linear relationship, which was too conservative and unreasonable. Investigators should gather more relevant experimental data to facilitate future improvements.
4. The PIDR of the corrugated steel plate sheathing CFS structure was less than the specification limit under the action of frequent, rare, and extremely rare earthquakes, and can therefore meet the requirements of multi-level seismic precautions. This will provide a reference for the seismic design of the structure under extremely rare conditions.
5. A reasonable CFS structural model was developed in OpenSees and the seismic performance parameters are evaluated by pushover analysis. These factors ($R = 6.5$ and $\Omega_0 = 3.0$) is appropriate for the perforated cold-formed steel framed shear wall systems using corrugated steel sheathing.

Author statement

Zhao Yan: Ideas, Methodology, Writing-original manuscript, reviewing. Yu Cheng: Writing-review & editing. Zhang Wenying: Formal analysis, Reviewing, Resources. Yu Shaole: Visualization. Du Xiuli: Software.

Declaration of competing interest

The authors declare that they have no known competing financial interests or personal relationships that could have appeared to influence the work reported in this paper.

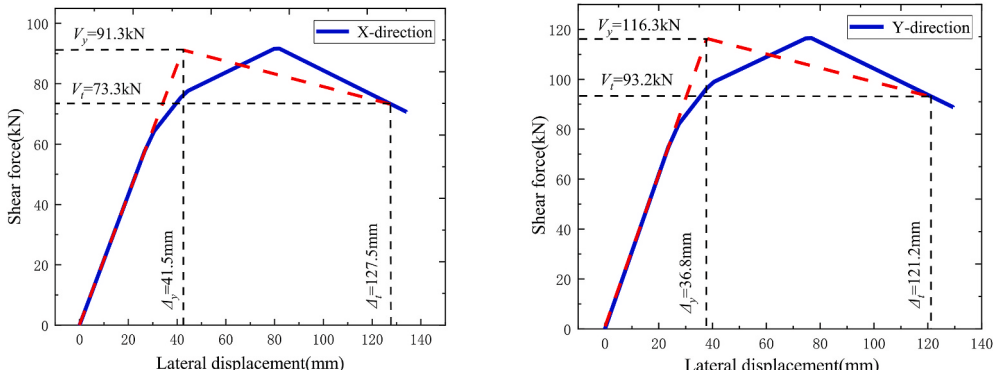


Fig. 30. Pushover curve of CFS structure.

Table 8

Response modification factor of CFS structure.

Specimens	X-direction	Y-direction
Δ_y (mm)	41.5	36.8
V_y (kN)	91.3	116.3
Δ_t (mm)	127.5	121.2
V_s (kN)	29.3	35.4
Ω_0	3.12	3.29
R_d	2.13	2.26
R	6.65	7.44

Data availability

Data will be made available on request.

Acknowledgements

This research was supported by National Natural Science Foundation of China No. 52008008, the Beijing Natural Science Foundation No. 8204053, and the Beijing Municipal Education Commission No. KM202010005029. The research was also partially sponsored by Shanghai Rising-Star Program No.21QB1406400. Any opinions, findings, conclusions, or recommendations expressed in this article are those of the authors and do not necessarily reflect the views of the sponsors.

References

- [1] T.S. Tarpy, Shear resistance of steel-stud wall panels, in: Proceeding of 5th International Specialty Conference on Cold-Formed Steel Structures, University of Missouri-Rolla, St. Louis, MO, USA, 1980, pp. 331–348.
- [2] T.S. Tarpy, J.D. Girard, Shear resistance of steel-stud wall panels, in: Proceeding of 6th International Specialty Conference on Cold-Formed Steel Structures, University of Missouri-Rolla, St-Louis, MO, USA, 1982, pp. 449–465.
- [3] R. Serrette, H. Nguyen, G. Hall, Shear Wall Values for Light Weight Steel Framing, Department of Civil Engineering, Santa Clara University, Santa Clara, CA, 1996.
- [4] R. Serrette, J. Encalada, M. Juadines, H. Nguyen, Static racking behavior of plywood, OSB, gypsum, and fiberboard walls with metal framing, *J. Struct. Eng. ASCE* 123 (8) (1997) 1079–1086.
- [5] A.J. Salenovich, J.D. Dolan, W.S. Easterling, Racking performance of long steel-frame shear walls, in: Proceeding of 15th International Specialty Conference on Cold-Formed Steel Structures, University of Missouri-Rolla, St. Louis, MO, USA, 2000, pp. 471–480.
- [6] P. Liu, K.D. Peterman, B.W. Schafer, Impact of construction details on OSB-sheathed cold-formed steel framed shear walls, *J. Constr. Steel Res.* 101 (2014) 114–123.
- [7] C. Yu, Shear resistance of cold-formed steel framed shear walls with 0.686 mm, 0.762 mm, and 0.838 mm steel sheet sheathing, *Eng. Struct.* 32 (6) (2010) 1522–1529.
- [8] W. Zhang, X. Xu, Y. Liu, et al., High-strength cold-formed steel framed shear wall with steel sheet sheathing[J], *Thin-Walled Struct.* 162 (2021), 107584.
- [9] Y. Shi, Z. Luo, Y. Xu, et al., Experimental study on the seismic behavior of high-performance cold-formed steel plate shear walls[J], *Eng. Struct.* 251 (2022), 113552.
- [10] L.A. Filop, D. Dubina, Performance of wall-stud cold-formed shear panels under monotonic and cyclic loading: Part I: experimental research, *Thin-Walled Struct.* 42 (2) (2004) 321–338.
- [11] B. Stojadinovic, S. Tipping, Structural testing of corrugated sheet steel shear walls, in: Proceedings of 19th International Specialty Conference on Cold-Formed Steel Structures, University of Missouri-Rolla, St Louis, Missouri, USA, 2008, pp. 425–439.
- [12] M. Waiel, K. Vail, Cyclic lateral load behavior of CFS walls sheathed with different materials, *Thin-Walled Struct.* 96 (2015) 328–336.
- [13] C. Yu, Z. Huang, H.D. Vora, et al., Cold-formed steel framed shear wall assemblies with corrugated sheet steel sheathing, in: Proceedings of the Annual Stability Conference Structural Stability, Research Council, Phoenix, AZ, USA, 2009, pp. 257–276.
- [14] G. Yu, Cold-formed Steel Framed Shear Wall Sheathed with Corrugated Sheet Steel, M.S. thesis, Dept. of Engineering Technology, University of North Texas, 2013.
- [15] C. Yu, W. Zhang, G. Yu, et al., Cold-formed steel shear wall using corrugated steel sheathing with slits, *J. Struct. Eng.* 144 (8) (2018), 04018111.
- [16] W. Zhang, M. Mahdavian, C. Yu, Different slit configuration in corrugated sheathing of cold-formed steel shear wall, *J. Constr. Steel Res.* 150 (2018) 430–441.
- [17] IBC, International Building Code. International Code Council, IBC, Washington, DC, 2018.
- [18] E.F. Gad, Performance of Brick-Veneer Cold-Formed Steel-Framed Domestic Structures Subjected to Earthquake Loading, Department of Civil and Environment Engineering, University of Melbourne, Australia, 1997.
- [19] E.F. Gad, C.F. Duffield, A.M. Chandler, G. Stark, Testing of cold-formed steel-framed domestic structures, in: The Proceedings of the 11th European Conference on Earthquake on Mechanics of Structures and Materials, 1998, pp. 323–329. Melbourne, Australia.
- [20] E.F. Gad, Adrian M. Chandler, Colin F. Duffield, Lateral behavior of plasterboard-clad residential steel frames, *J. Struct. Eng.* 125 (1) (1999) 32–39.
- [21] D. Dubina, Behavior and performance of cold-formed steel-framed houses under seismic action, *J. Constr. Steel Res.* 64 (2008) 896–913.
- [22] D. Dubina, Structural analysis and design assisted by testing of cold-formed steel structures, *Thin-Walled Struct.* 46 (2008) 741–764.
- [23] L. Fiorino, V. Macillo, R. Landolfo, Shake table tests of a full-scale two-floor sheathing-braced cold-formed steel building, *Eng. Struct.* 151 (2017) 633–647.
- [24] K.D. Peterman, M.J.J. Stehman, S.G. Buonopane, et al., Seismic performance of full-scale cold-formed steel buildings, in: Tenth U.S. National Conference on Earthquake Engineering, Frontiers of Earthquake Engineering, Anchorage Alaska, 2014. July 21–25.
- [25] K.D. Peterman, M.J.J. Stehman, R.L. Madsen, et al., Experimental seismic response of a full-scale cold-formed steel-framed building. I: system-level response, *J. Struct. Eng.* 142 (12) (2016), 04016127.
- [26] K.D. Peterman, M.J.J. Stehman, R.L. Madsen, et al., Experimental seismic response of a full-scale cold-formed steel-framed building. II: subsystem-level response, *J. Struct. Eng.* 142 (12) (2016), 04016128.
- [27] B.W. Schafer, D. Ayhan, J. Leng, et al., Seismic response and engineering of cold-formed steel framed buildings, *Structures* 8 (2016) 197–212.
- [28] Tae-Wan Kim, Wilcoski James, Shake table tests of a cold-formed steel shear panel, *Eng. Struct.* 28 (2006) 1462–1470.
- [29] L. Fiorino, B. Bucciero, R. Landolfo, Shake table tests of three storey cold-formed steel structures with strap-braced walls, *Bull. Earthq. Eng.* 17 (7) (2019) 4217–4245.
- [30] Li, Y., Shen, Z., Yao, X., Ma, R., & Liu, F. Experimental investigation and design method research on low-rise cold-formed thin-walled steel framing buildings. *J. Struct. Eng.*, 139(5), 818–836.

- [31] J.H. Ye, L.Q. Jiang, Simplified analytical model and shaking table test validation for seismic analysis of midrise cold-formed steel composite shear wall building, *Sustainability* 10 (9) (2018) 3188.
- [32] X. Wang, E. Pantoli, T.C. Hutchinson, et al., Seismic performance of cold-formed steel wall systems in a full-scale building, *J. Struct. Eng.* 141 (10) (2015), 04015014.
- [33] ASCE, Minimum Design Loads and Associated Criteria for Buildings and Other Structures ASCE 7, American Society of Civil Engineers, Reston, Virginia, 2016.
- [34] Code for Seismic Design of Buildings: GB 50011—2001, China Architecture & Building Press, Beijing, 2001 (In Chinese).
- [35] Eurocode 8: Design of Structures for Earthquake Resistance. Part1: General Rules, Seismic Actions and Rules for Buildings European Standard EN1998-1: 2004, CEN., Brussels, 2004.
- [36] Seismic Ground Motion Parameters Zonation Map of China: GB 18036-2015, Standardization Administration of the People's Republic of China, Beijing, 2015 (In Chinese).
- [37] Metallic Material: Tensile Testing: Part I: Method at Room Temperature: GB/T228.1—2010, China Standard Press, Beijing, 2010 (In Chinese).
- [38] Load Code for the Design of Building Structure: GB50009-2012, China Architecture & Building Press, Beijing, 2018 (In Chinese).
- [39] Technical Specification for Low-Rise Cold-Formed Thin-Walled Steel Buildings. JGJ 227-2011, China Architecture & Building Press, Beijing, 2018 (In Chinese).
- [40] FEMA, FEMA P695 Quantification of Building Seismic Performance Factors, Federal Emergency Management Agency, Washington, D.C., 2009.
- [41] AC322, AC322 Prefabricated, Cold-Formed, Steel Lateral-Force-Resisting Vertical Assemblies, International Code Council Evaluation Service, Washington, DC, 2013.
- [42] W. Zhang, M. Mahdavian, Y. Li, C. Yu, Experiments and simulations of cold-formed steel wall assemblies using corrugated steel sheathing subjected to shear and gravity loads, *J. Struct. Eng.* 143 (3) (2016), 04016193.
- [43] W. Zhang, C. Yu, M. Mahdavian, Seismic performance of cold-formed steel shear walls using corrugated sheathing with slits, *J. Struct. Eng.* 145 (4) (2019).
- [44] W. Zhang, M. Mahdavian, Y. Li, et al., Seismic performance evaluation of cold-formed steel shear walls using corrugated steel sheathing, *J. Struct. Eng.* 143 (11) (2017), 04017151.
- [45] X.Y Liu, Shear performance of cold-formed steel shear walls sheathed with corrugated steel sheet, Beijing University of Technology, Beijing, 2022 (In Chinese).
- [46] ATC-3-06, Tentative Provisions for the Development of Seismic Regulations for Buildings, Applied Technology Council, National Centre for Earthquake Engineering Research, USA, 1978.
- [47] ASCE 41-13: seismic evaluation and retrofit rehabilitation of existing buildings, in: Proceedings of the SEAOC, 2012.
- [48] N. Newmark, W. Hall, Earthquake Spectra and Design, Earthquake Engineering Research Inst., Berkeley, CA, 1982.